Ferromagnetism in $CaMn_{1-x}Ir_xO_3$

2008 J. Phys.: Condens. Matter 20 235242

(http://iopscience.iop.org/0953-8984/20/23/235242)

J. Phys.: Condens. Matter **20** (2008) 235242 (7pp) doi:10.1088/0953-8984/20/23/235242

Ferromagnetism in $CaMn_{1-x}Ir_xO_3$

S Mizusaki[1,6], J Sato[1], T Taniguchi[1], Y Nagata[1], S H Lai[2], M D Lan[2], T C Ozawa[3], Y Noro[4] and H Samata[5]

[1] College of Science and Engineering, Aoyama Gakuin University, Fuchinobe, Sagamihara, Kanagawa 157-8572, Japan
[2] Department of Physics, National Chung Hsing University, Taichung 402, Taiwan, Republic of China
[3] Nanoscale Materials Center, National Institute for Materials Science, Namiki, Tsukuba, Ibaraki 305-0044, Japan
[4] Kawazoe Frontier Technologies, Co. Ltd, Kuden, Sakae, Yokohama, Kanagawa 931-113, Japan
[5] Faculty of Maritime Sciences, Kobe University, Fukaeminami, Higashinada, Kobe, Hyogo 658-0022, Japan

E-mail: smizusaki@ee.aoyama.ac.jp

Received 14 November 2007, in final form 1 April 2008
Published 13 May 2008
Online at stacks.iop.org/JPhysCM/20/235242

Abstract

The crystallographic, magnetic, and electric properties of $CaMn_{1-x}Ir_xO_3$ ($0 \leqslant x \leqslant 0.6$) were investigated. The lattice constants increase with increasing content of Ir. Specimens of $0.05 \leqslant x \leqslant 0.2$ show antiferromagnetic behavior; however, ferromagnetism is observed for specimens of $0.3 \leqslant x \leqslant 0.6$. T_N decreases as the Ir content increases. T_N is superseded by T_C without passing 0 K and T_C continues to increase in the ferromagnetic composition range. The effective moment μ_{eff} decreases as the Ir content increases. The Weiss temperature is negative for small x; however, it continues to increase while changing its sign at about $x = 0.3$. The results were explained by assuming a mixed valence state of Mn^{3+}, Mn^{4+}, Ir^{4+}, and Ir^{5+} ions. The composition dependence of μ_{eff} could be explained qualitatively using the ion fractions estimated from the Ir content dependence of the unit cell volume. Experimental results suggest the coexistence of antiferromagnetic and ferromagnetic phases. When the volume fraction of the ferromagnetic phase dominates that of the antiferromagnetic phase, the system seems to show ferromagnetism.

1. Introduction

The colossal magnetoresistance (CMR) observed in hole-doped perovskite-type manganites [1] has attracted renewed interest in perovskite-type manganites, and extensive studies have been conducted on these compounds. The end member $CaMnO_3$ is an antiferromagnetic insulator with a Néel temperature $T_N = 120$ K [2–4]. The nominal valence of Mn ions in stoichiometric $CaMnO_3$ is 4+. When Ca^{2+} is replaced by ions with a valence larger than 2+, such as La^{3+}, the Mn^{3+} ion is introduced into the matrix. The Mn^{3+} ion is also introduced by a partial substitution of Mn ions by a cation with a valence larger than 4+. Studies performed from the former viewpoint for $Ln_xCa_{1-x}MnO_3$ (Ln = lanthanides) revealed that holes are introduced by Ln doping and move from Mn^{4+} to Mn^{3+} ions dominating the transport. The mobile holes simultaneously mediate the ferromagnetic double-exchange interaction. At the same time, certain 3d electron-orbital configurations of Mn ions favor superexchange interactions and lead to the formation of antiferromagnetic or ferromagnetic insulating phases [5]. The coexistence of a ferromagnetic phase and an antiferromagnetic insulating phase has been reported for various manganite systems [6–9].

Studies from the latter viewpoint were conducted for the $CaMn_{1-x}Ru_xO_3$ system [10–14]. In this system, Ru doping to antiferromagnetic $CaMnO_3$ mediates ferromagnetic interactions and ferromagnetic clusters are formed in specimens of $x \geqslant 0.08$. The ferromagnetic clusters are linked at about $x = 0.2$, and the system becomes metallic. It was pointed out that the predominant valence state of Ru is 5+ for the composition of $x \approx 0.5$, contrary to the expectation that the valence of Ru is 4+. Therefore, the replacement of Mn^{4+} by Ru^{5+} creates Mn^{3+} in order

[6] Author to whom any correspondence should be addressed.

to compensate the charge unbalance and then leads to the appearance of a ferromagnetic double-exchange interaction between Mn^{4+} and Mn^{3+} ions. In addition, the ferromagnetic superexchange interactions between Ru^{5+} and Mn^{3+} ions also enhance the ferromagnetism. These features are enhanced with increasing content of Ru, and the Curie temperature reaches the maximum (210 K) at $x = 0.3$–0.4. In the studies, it was also suggested that the major ferromagnetic phase coexists with other magnetically ordered phases as in the case of $Ln_xCa_{1-x}MnO_3$ (Ln = lanthanide) [13]. When we take these results into account, it is expected that new ferromagnetic oxides can be found in manganites by the partial substitution of the Mn site by cations with a valence larger than 4+.

From this viewpoint, we have studied the $CaMn_{1-x}M_xO_3$ (M = pentavalent 4d or 5d transition metal ions) system. In general, the spatially extended d orbitals of 4d and 5d transition metal ions enhance crystal-field splitting and the ligand oxygen leads to strong electron–lattice coupling. Therefore, drastic changes in the magnetic and transport properties are expected for $CaMn_{1-x}M_xO_3$ systems. Among 5d transition metal ions, iridium, Ir, is very interesting because it has been reported to take valences of 4+ and 5+ in oxides such as $Ln_2Ir_2O_7$ and Ln_3IrO_7, respectively [15–27]. Therefore, when some Mn ions are replaced by Ir ions in the $CaMn_{1-x}Ir_xO_3$ system, ferromagnetism is likely to occur due to the mixed valence state of Ir ions. In this study, the crystallographic, magnetic, and electric properties of the $CaMn_{1-x}Ir_xO_3$ system were examined in detail, and the reason for the occurrence of ferromagnetism was discussed.

2. Experimental details

Polycrystalline specimens of $CaMn_{1-x}Ir_xO_3$ ($0 \leqslant x \leqslant 0.7$) were prepared by the usual solid-state reaction method using high-purity reagents of $CaCO_3$ (99.9%), Mn_2O_3 (99.9%) and IrO_2 (99.9%). $CaCO_3$ was used after annealing the powder at 500 °C for 24 h. A stoichiometric amount of the reagents was mixed in an agate mortar, and after being pressed into a pellet, the mixture was calcined at temperatures between 900 and 1200 °C for 10 h. The mixing and calcination were repeated every 50 °C between 900 and 1200 °C. After final sintering at 1200 °C the specimens were annealed at 600 °C for 36 h in an oxygen atmosphere.

The crystal structure was characterized by x-ray powder diffraction using Cu Kα radiation and subsequent refinement by the Rietveld method. The magnetic property was characterized using a superconducting quantum interference device (SQUID) magnetometer at temperatures between 5 and 350 K under an applied magnetic field up to 70 kOe. The electrical resistivity was measured using a DC four-probe method. Electrical contact was established by attaching gold leads onto the surface of the specimen using a gold paste.

3. Results and discussion

3.1. Crystallographic properties

The x-ray powder diffraction profiles for specimens of $CaMn_{1-x}Ir_xO_3$ ($0 \leqslant x \leqslant 0.7$) are shown in figure 1. No

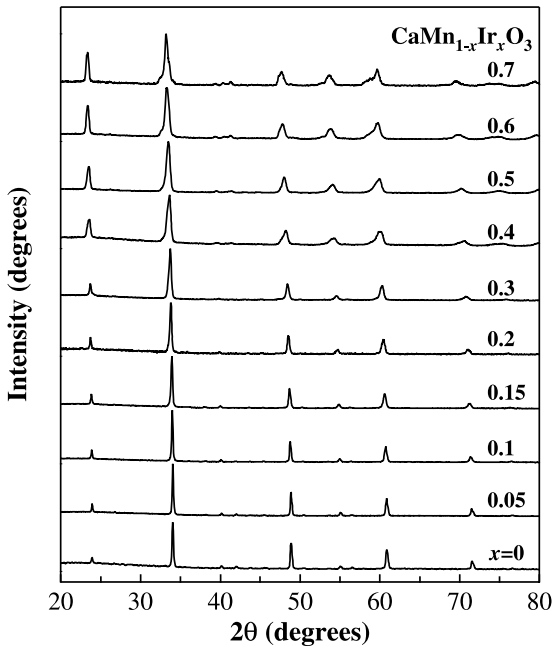

Figure 1. X-ray powder diffraction profiles for specimens of $CaMn_{1-x}Ir_xO_3$ ($0 \leqslant x \leqslant 0.7$).

trace of raw materials or a secondary phase was observed for specimens of $0 \leqslant x \leqslant 0.6$; however, traces of an impurity phase, such as Ca_2IrO_4, were observed for the specimen of $x = 0.7$. The diffraction data except that of $x = 0.7$ could be refined assuming an orthorhombic structure of the space group $Pbnm$. The reliable factors R_{wp} and R_I of the refinements were in the range of 6.6–12.4 and 5.7–12.9, respectively. The refined lattice parameters and the cubic root of the pseudo-cubic unit cell volume of $CaMn_{1-x}Ir_xO_3$ are shown in figures 2(a) and (b) as a function of Ir content x. All the lattice parameters increase as the content of Ir increases. This seems to be due to the fact that the Ir ion has a larger ionic radius than the Mn ion. Ion species and their fractions were estimated using the Mn content dependence of the unit cell volume. In the calculation, an empirical formula

$$V^{1/3} = 1.999r_i + 0.420\,65, \tag{1}$$

which was obtained from the data of the unit cell volumes of isomorphic oxides $CaMO_3$ (M = Ti, V, Mn, Fe, Ge, Zr, Nb, Ru, Sn, Ir, Pb) and the ionic radii of M ions [28–30], was used. Here, V and r_i are the unit cell volume and ionic radius of the M ion, respectively. When the Ir ion replaces Mn as Ir^{4+}, the average ionic radius r_{im} of the M ion is calculated by the relation

$$r_{im} = 0.053(1 - x) + 0.0625x, \tag{2}$$

where x is the Ir content and 0.053 and 0.0625 are the ionic radii of Mn^{4+} and Ir^{4+} ions, respectively. The Ir content dependence of the unit cell volume calculated using relations (1) and (2) is shown in figure 2(b) as 'calculation-1'. It is seen that the result of the calculation deviates considerably from the experimental result, suggesting the existence of other ions with larger ionic radii than Mn^{4+} and Ir^{4+}. It is commonly

Table 1. Ion fractions estimated from the relation between the average ionic radius r_{im} and the Ir content dependence of the unit cell volume of $CaMn_{1-x}Ir_xO_3$, ion pair fractions, and effective magnetic moment μ_{eff}.

x	Mn^{3+}	Mn^{4+}	Ir^{4+}	Ir^{5+}	Mn^{3+}–Mn^{4+} fraction[a]	Mn^{4+}–Ir^{4+} fraction[a]	Estimated μ_{eff} (μ_B)	Experimental μ_{eff} (μ_B)
0	0	1	0	0	0	0	3.87	3.81
0.05	0.050	0.900	0	0.050	0.284	0	3.83	3.84
0.10	0.094	0.806	0.006	0.094	0.505	0.036	3.79	3.68
0.15	0.134	0.712	0.017	0.133	0.677	0.996	3.74	3.64
0.20	0.169	0.632	0.032	0.168	0.800	0.183	3.68	3.56
0.30	0.224	0.477	0.077	0.223	0.915	0.398	3.55	3.32
0.40	0.260	0.340	0.140	0.260	0.884	0.595	3.40	3.12
0.50	0.276	0.224	0.224	0.276	0.742	0.672	3.22	3.07
0.60	0.273	0.127	0.327	0.273	0.520	0.549	3.00	2.71

[a] Values are relative fractions calculated using the formula $N_{AB} = zN_AN_B/(N_A + N_B)$, where N_A, N_B, N_{AB}, and z are the fractions of A and B ions, the number of the A–B pair, and the number of nearest-neighbor metal ions of A ion, respectively.

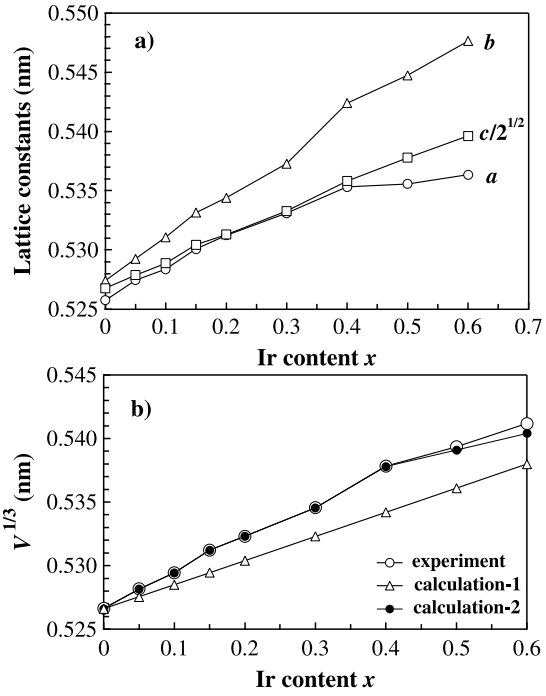

Figure 2. Ir content dependence of (a) the refined lattice parameters and (b) the cubic root of the pseudo-cubic unit cell volume of $CaMn_{1-x}Ir_xO_3$ ($0 \leqslant x \leqslant 0.6$).

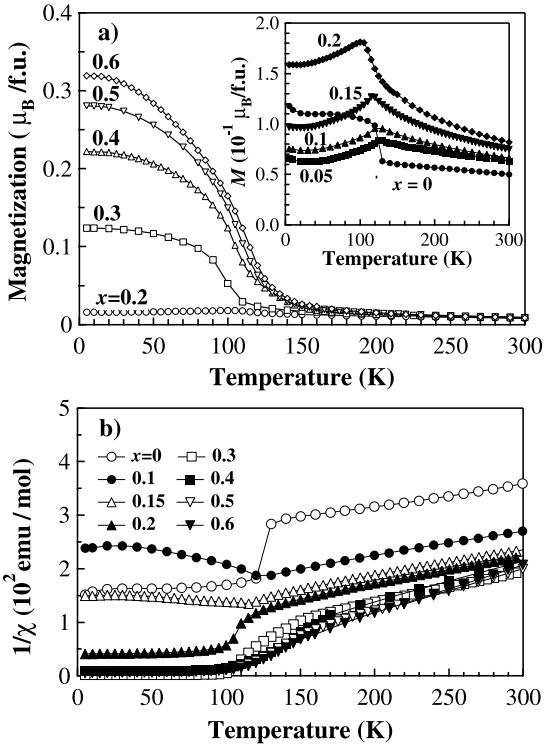

Figure 3. (a) Temperature dependence of the magnetization and (b) the reciprocal magnetic susceptibility χ^{-1} measured for $CaMn_{1-x}Ir_xO_3$ ($0 \leqslant x \leqslant 0.6$) under an applied field of 10 kOe.

understood that iridium ions are stabilized in the tetravalent state in most oxides; however, the existence of the pentavalent iridium Ir^{5+} has also been reported for iridium oxides such as $KIrO_3$, La_2LiIrO_6, and A_2LnIrO_6 (A = Sr, Ba; Ln = Sc, Y, La, Lu) [31–35]. Therefore, it is likely that Ir ions exist as Ir^{4+} and Ir^{5+} in the $CaMn_{1-x}Ir_xO_3$ system. Assuming the mixed valence state of Mn^{3+}, Mn^{4+}, Ir^{4+}, and Ir^{5+} ions, the fractions of each ion were estimated using the relation (1), the composition dependence of unit cell volume, and the average ionic radius r_{im}. In this case r_{im} is represented by

$$r_{im} = 0.0645y + 0.053(1 - x - y) + 0.0625(x - y) + 0.057y. \quad (3)$$

where 0.0645, 0.053, 0.0625, and 0.057 nm are the radii of Mn^{3+}, Mn^{4+}, Ir^{4+}, and Ir^{5+} ions, respectively, and y is the fraction of Mn^{3+} ions. In this estimation, it has been assumed that the fraction of the Mn^{3+} ion is in principle the same as that of the Ir^{5+} ion but smaller than the Ir content x and the Mn^{4+} fraction. The result of the estimation is listed in table 1, and the Ir content dependence of the unit cell volume calculated using the relations (1) and (3) is shown in figure 2(b) as 'calculation-2'. It is clearly seen that the estimated fractions reproduce the relation between the Ir content and the cubic root of the unit cell volume.

3.2. Magnetic properties

Figure 3(a) shows the temperature dependence of the magnetization M measured for $CaMn_{1-x}Ir_xO_3$ ($0 \leqslant x \leqslant 0.6$)

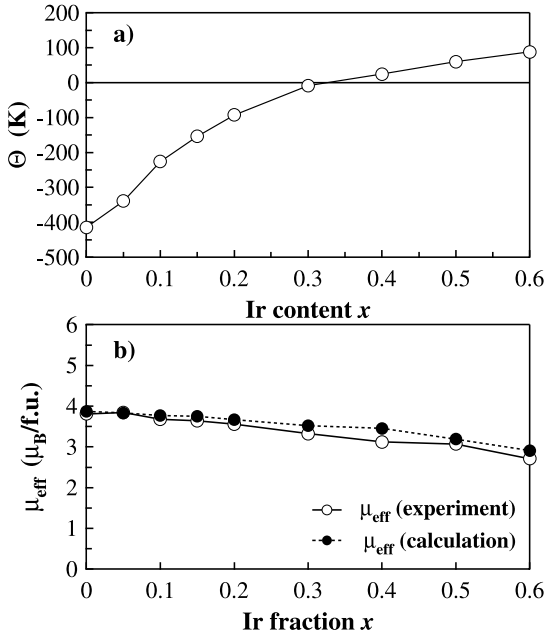

Figure 4. Ir content dependence of (a) the Weiss temperature Θ and (b) the effective magnetic moment $\mu_{\rm eff}$ deduced from the Curie constant obtained for $\chi^{-1}(T)$ data at higher temperatures.

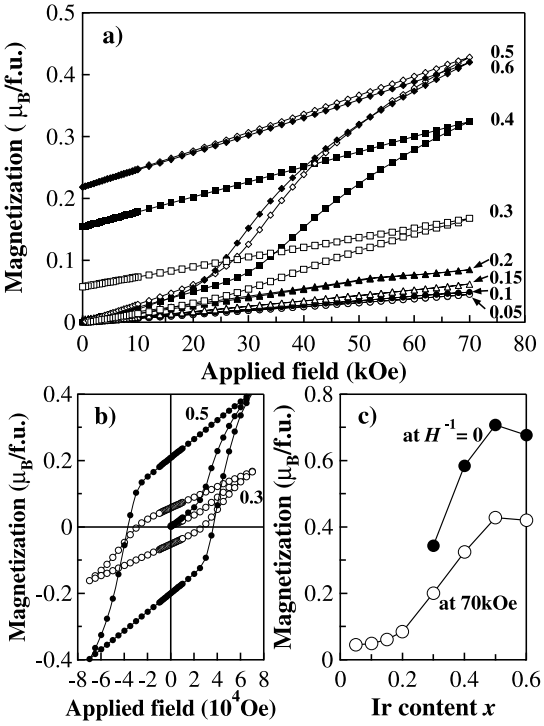

Figure 5. (a) Magnetic-field dependence of the magnetization measured for $CaMn_{1-x}Ir_xO_3$ ($0 \leqslant x \leqslant 0.6$) at 5 K, (b) magnetic hysteresis curves for specimens of $x = 0.3$ and 0.5, and (c) Ir content dependence of the magnetization at 70 kOe (μ_{70}) and the estimated magnetization (μ_∞) at $H^{-1} = 0$.

under an applied field of 10 kOe. $M(T)$ values of the specimens of $x < 0.3$ show antiferromagnetic characteristics and have peaks in the vicinity of 100 K. On the other hand, those of $x \geqslant 0.3$ show ferromagnetic characteristics. The temperature dependence of the reciprocal magnetic susceptibility χ^{-1} is shown in figure 3(b). The Weiss temperature Θ and Curie constant C were determined by fitting the linear portion of the $\chi^{-1}(T)$ data to the Curie–Weiss law. Figure 4 shows the Ir content dependence of (a) the Weiss temperature Θ and (b) the effective magnetic moment $\mu_{\rm eff}$ deduced from the Curie constant. Θ is negative for specimens of $x < 0.3$; however, Θ increases as the Ir content increases, and, after changing its sign from negative to positive at about $x = 0.3$, it continues to increase up to $x = 0.6$. On the other hand, $\mu_{\rm eff}$ decreases as the Ir content increases, suggesting that ions with smaller magnetic moments than that of Mn^{4+} are introduced by Ir doping. This is consistent with the fact pointed out in the previous section.

Figure 5(a) shows the magnetic-field dependence of the magnetization for specimens of $CaMn_{1-x}Ir_xO_3$ ($0.05 \leqslant x \leqslant 0.6$) at 5 K. The $M(H)$ curves for specimens of $0.05 \leqslant x \leqslant 0.2$ show almost linear temperature dependence. Specimens of $x \geqslant 0.3$ show a hysteresis, indicating that the specimens of these compositions are ferromagnetic; however, the magnetization does not saturate even at 70 kOe. Since no saturation was observed in the $M(H)$ curves for specimens of $x \geqslant 0.3$, the magnetization at $H = \infty$ is estimated instead of the saturation magnetization. Figure 5(b) shows magnetic hysteresis curves for specimens of $x = 0.3$ and 0.5. Although the magnetization is not saturated up to 70 kOe and the intrinsic coercive force cannot be characterized, it is evident that these specimens have considerably large coercive forces of more than 30 kOe. Figure 5(c) shows the Ir content dependence of the μ_∞ at $H = \infty$ along with the magnetization μ_{70} at 70 kOe. The magnetization at $H = \infty$ was estimated by extrapolating the linear portion of the $M(H^{-1})$ curve to $H^{-1} = 0$. The magnetization increases remarkably above $x = 0.3$; however, it tends to be saturated for specimens of $x \geqslant 0.5$. The values of μ_∞ and μ_{70} are one order of magnitude smaller than the effective moment $\mu_{\rm eff}$. The possible reason for this discrepancy as well as the characteristic $M(H)$ curve will be discussed later.

After taking the $M(T)$, $\Theta(x)$, and $M(H)$ data into consideration we concluded that the specimens of $x < 0.3$ are antiferromagnetic and those of $x \geqslant 0.3$ are ferromagnetic. The Néel temperature $T_{\rm N}$ and Curie temperature $T_{\rm C}$, which are determined from the $M(T)$ data are shown in figure 6 as a function of the Ir content x. Here, $T_{\rm N}$ was defined as the peak temperature observed in the $M(T)$ data for antiferromagnetic specimens and $T_{\rm C}$ was defined as an inflection point observed in the $M(T)$ data for ferromagnetic specimens (the inflection point was determined from the temperature dependence of dM/dT). $T_{\rm N}$ decreases as the Ir content increases; however, $T_{\rm C}$ increases with increasing content of Ir. It is evident that there is a considerable difference between $T_{\rm C}$ and Θ for specimens with a ferromagnetic composition. In addition, it is very strange that $T_{\rm N}$ is superseded by $T_{\rm C}$ without passing 0 K.

Here, we consider the experimental results from the viewpoint of the mixed valence model proposed in section 3.1, in which the coexistence of Mn^{3+}, Mn^{4+}, Ir^{4+} and Ir^{5+} ions is assumed. Following the qualitative consideration of

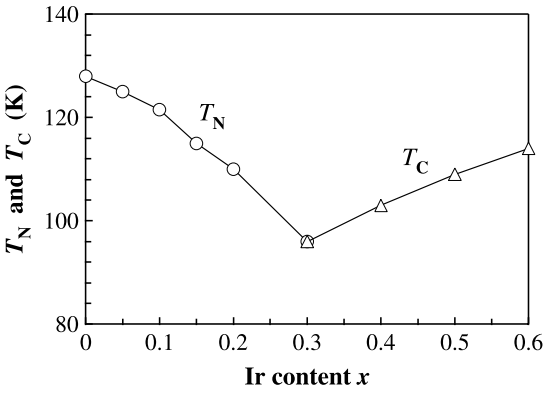

Figure 6. Ir content dependence of the Néel temperature T_N and the Curie temperature T_C of $CaMn_{1-x}Ir_xO_3$ ($0 \leqslant x \leqslant 0.6$).

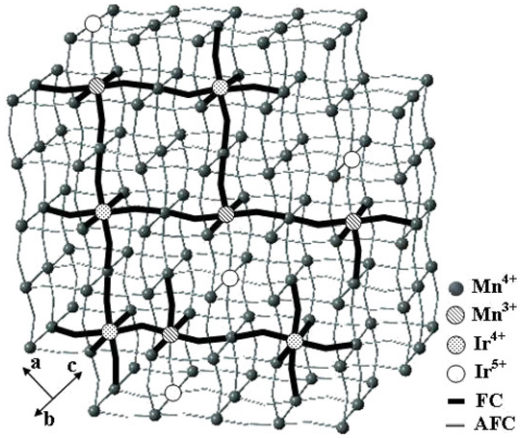

Figure 7. Formation of ferromagnetic clusters in the crystal lattice of $CaMn_{1-x}Ir_xO_3$. Oxygen ions have been omitted so that the cations can be clearly seen.

Goodenough [36], antiferromagnetic superexchange interaction is expected for $Mn^{4+}(3d^3)$–O–$Mn^{4+}(3d^3)$, $Mn^{3+}(3d^4)$–O–$Ir^{4+}(5d^5)$, and $Ir^{4+}(5d^5)$–O–$Ir^{4+}(5d^5)$ paths, and a ferromagnetic superexchange interaction is expected for the Mn^{3+}–O–Mn^{4+}, Mn^{4+}–O–Ir^{4+}, and Mn^{3+}–O–Mn^{3+} paths. In particular, not only the superexchange interaction but also a ferromagnetic double-exchange interaction is expected for Mn^{3+}–Mn^{4+} pairs. As mentioned in section 1, most Ir ions are considered to be substituted for Mn^{4+} in $CaMnO_3$ as Ir^{5+} in the case of specimens with a small Ir content. In this case, nearest-neighbor Mn^{4+} ions must change to Mn^{3+} ions to maintain the charge neutrality. In addition, since it was reported that the Ir^{5+} ion with a low-spin t_{2g}^4 configuration has a non-magnetic ground state [34, 35], the Ir^{5+} ion should be treated as a non-magnetic ion. Therefore, as shown in figure 7, when Ir is substituted for Mn in $CaMnO_3$, ferromagnetic clusters are formed in the antiferromagnetic matrix via ferromagnetic Mn^{3+}–Mn^{4+}, Mn^{4+}–Ir^{4+}, and Mn^{3+}–Mn^{3+} interactions. As reported in section 1, the coexistence of ferromagnetic and antiferromagnetic phases was found in many manganites [6–9]. Presumably, a similar situation is realized in the $CaMn_{1-x}Ir_xO_3$ system. In the specimens with smaller Ir contents ($x < 0.3$), the volume fraction of an antiferromagnetic region seems much larger than that of a ferromagnetic region. In this case, when T_N is higher than T_C, the specimens would show antiferromagnetic behavior below T_N having ferromagnetic clusters inside. The fraction of a ferromagnetic cluster increases as the Ir content increases and the clusters percolate, forming larger ferromagnetic regions. When the volume fraction of the ferromagnetic region dominates that of the antiferromagnetic region and T_C is higher than T_N, the system shows ferromagnetic behavior below T_C. Furthermore, T_N will be superseded by T_C without passing 0 K in this case. This type of crossover between T_N and T_C is also observed in manganite such as $La_{1-x}Ca_xMnO_3$ [37, 38]. As mentioned above, the Θ values of ferromagnetic specimens ($x \geqslant 0.3$) are considerably lower than T_C. This suggests that antiferromagnetic regions still remain in the major ferromagnetic regions. As shown in table 1, the relative fraction of the ferromagnetic Mn^{3+}–Mn^{4+} pair increases remarkably in the specimens with a small Ir content, and after reaching the maximum at about $x = 0.3$, it tends to decrease for specimens of $x > 0.3$; however, T_C and Θ continue to increase above $x = 0.3$. On the other hand, the Mn^{4+}–Ir^{4+} pair fraction continues to increase up to $x = 0.5$. Therefore, it is considered that the ferromagnetic Mn^{3+}–Mn^{4+} interaction makes a major contribution to the initial formation of ferromagnetic clusters in specimens with a small Ir composition and the ferromagnetic Mn^{4+}–Ir^{4+} interaction takes over the key role in the formation of the ferromagnetic phase in specimens with a larger Ir composition.

The effective magnetic moment μ_{eff} was calculated assuming the ionic fractions shown in table 1 and the magnetic moments of Mn^{3+}, Mn^{4+}, and Ir^{4+} (low-spin) ions as 4.89, 3.87, and 1.73 μ_B, respectively. The moment of Ir^{5+} was assumed to be zero. The result of the calculation is shown in figure 4(b). Although there is a slight difference between the experimental μ_{eff} and the results of calculation, the calculation explains the experimental result qualitatively. On the other hand, the moment μ_∞ estimated from the $M(H)$ curve is one order of magnitude smaller than the μ_{eff}. This seems to be caused by the coexistence of ferromagnetic and antiferromagnetic phases. When the antiferromagnetic phase exists in the major ferromagnetic phase, a sort of ferrimagnetism is established, and then the ferromagnetic moment μ_∞ is smaller than the effective moment μ_{eff} deduced from the Curie constant obtained for the higher temperature portion of the $\chi(T)$ data. Furthermore, De Gennes reported as a result of a study of perovskite-type manganites, such as $La_{1-x}Ca_xMnO_3$, that the ground state with canted-spin ferromagnetism is realized in a wide composition range when the superexchange interaction surpasses the double-exchange interaction, satisfying the condition $t_0 < 4|J|S^2$, where J, S, and t_0 are the exchange integral, spin, and coefficient of the transfer integral, respectively [39]. Therefore, as in the case of manganites, it is likely that the canted-spin ferromagnetism is realized in the $CaMn_{1-x}Ir_xO_3$ system at very low temperature. In this case, the experimental moment μ_∞ estimated from the $M(H)$ data would decrease more than the value that is calculated, assuming the parallel spin configuration of Mn and Ir ions.

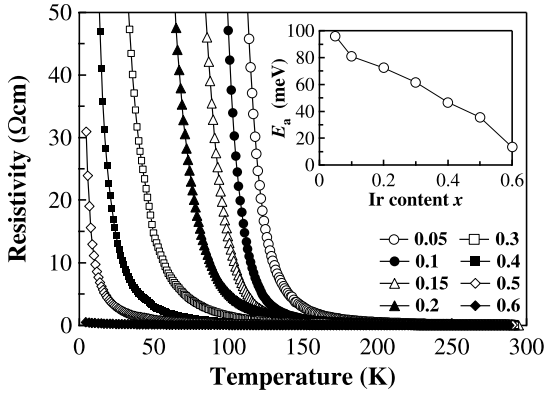

Figure 8. (a) Temperature dependence of the electrical resistivity measured for $CaMn_{1-x}Ir_xO_3$ ($0 \leqslant x \leqslant 0.6$) and (b) Ir content dependence of the activation energy E_a.

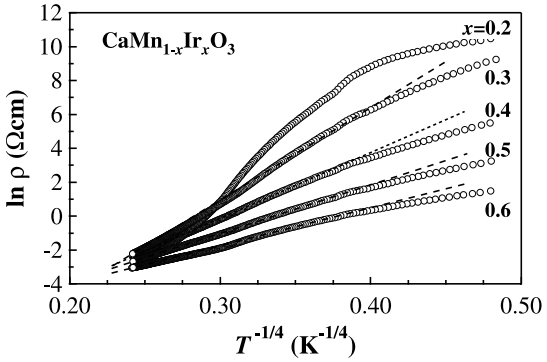

Figure 9. $T^{-1/4}$ dependence of the logarithmic resistivity for $CaMn_{1-x}Ir_xO_3$ ($0.2 \leqslant x \leqslant 0.6$). The dotted lines are the results of fitting using the relation $\rho = a\exp(T_0/T)^{1/4}$.

In addition to the magnetization, the coexistence of ferromagnetic and antiferromagnetic phases would have a serious influence on the $M(H)$ curve. As shown in figure 5(a), the threshold field for magnetization was very large, and no saturation was observed for $M(H)$ curves up to 70 kOe. This type of magnetization curve is often observed for ferromagnets with a relatively large magnetic anisotropy. However, a large magnetic anisotropy cannot be expected for Mn^{3+}, Mn^{4+}, and Ir^{4+} ions because of their electronic state. When ferromagnetic and antiferromagnetic phases coexist in the specimens, it is likely that the ferromagnetic spins in the vicinity of the interface between the ferromagnetic and antiferromagnetic phases will be pinned by the spins in the antiferromagnetic phase and the threshold field for magnetization will become large.

3.3. Electric properties

Figure 8 shows the temperature dependence of the electrical resistivity measured for $CaMn_{1-x}Ir_xO_3$ ($0 \leqslant x \leqslant 0.6$). All specimens show semiconductor-like behavior, and the resistivity increases as the temperature decreases. The $\rho(T)$ at higher temperatures could be fitted by the activation-type formula, which is given by $\rho(T) = \rho_0 \exp(E_a/k_BT)$, where ρ, E_a, and k_B are the constant, the activation energy, and the Boltzmann's constant, respectively. The activation energy E_a is shown in the inset of figure 8 as a function of Ir content x. E_a shows an almost linear decrease as the Ir content x increases; however, a semiconductor–metal transition is not observed up to $x = 0.7$. Although specimens of $x \geqslant 0.8$ cannot be synthesized under ambient pressure, they are expected to have metallic conduction. Figure 9 shows the $T^{-1/4}$ dependence of the logarithmic resistivity $\ln\rho$ for $CaMn_{1-x}Ir_xO_3$. A linear $T^{-1/4}$ dependence is observed for specimens of $x \geqslant 0.3$ in the range of $T^{-1/4} = 0.25$–0.38. It is well known that, in the insulating specimens with strong inhomogeneity, the carrier localizes spatially at states with various energy. When there are states for which a carrier can be reached with the help of a phonon, hopping conduction occurs at a finite temperature. This phenomenon is called variable-range hopping (VRH). In the n-dimensional VRH, the logarithmic resistivity $\ln\rho$ is proportional to $T^{-1/(n+1)}$ [40]. The linear $T^{-1/4}$ dependence observed for specimens of $x \geqslant 0.3$ suggests that a three-dimensional variable-range hopping (VRH) occurs in these specimens. In these compositions, the coexistence of ferromagnetic and antiferromagnetic phases was suggested through studies of magnetic properties. Presumably, the coexistence of two magnetic phases introduces inhomogeneity, and VRH conduction then occurs.

4. Conclusion

The crystallographic, magnetic, and electric properties of $CaMn_{1-x}Ir_xO_3$ ($0 \leqslant x \leqslant 0.6$) were investigated. The lattice constants and the unit cell volume increase as the Ir content increases. Specimens of $x = 0.05$–0.2 show antiferromagnetic properties; however, ferromagnetism appears at about $x = 0.3$ and persists in the range of $x = 0.3$–0.6. T_N decreases with an increasing Ir content ($0 \leqslant x \leqslant 0.2$), but T_C increases in the ferromagnetic composition range of $0.3 \leqslant x \leqslant 0.6$. In addition, T_N is superseded by T_C without passing 0 K. The effective moment μ_{eff} decreases monotonously with increasing content of Ir. The Weiss temperature is negative for specimens of $x < 0.3$; however, it increases as the Ir content increases and changes its sign at about $x = 0.3$. The experimental results were explained assuming a mixed valence state in which Mn^{3+}, Mn^{4+}, Ir^{4+}, and Ir^{5+} ions coexist. The fraction of each ion was estimated from the Ir content dependence of the unit cell volume. The composition dependence of μ_{eff} could be explained qualitatively using the estimated ion fractions and the theoretical moment of Mn^{3+}, Mn^{4+}, and Ir^{4+} ions. However, the ferromagnetic moment μ_∞ estimated from the $M(H)$ data is one order of magnitude smaller than μ_{eff}, suggesting that the specimen is not fully ferromagnetic. This was attributed to the coexistence of ferromagnetic and antiferromagnetic phases. The ferromagnetic phase is considered to be formed by ferromagnetic Mn^{3+}–Mn^{4+}, Mn^{4+}–Ir^{4+}, and Mn^{3+}–Mn^{3+} interactions, and the antiferromagnetic phase is formed by antiferromagnetic Mn^{4+}–Mn^{4+}, Mn^{3+}–Ir^{4+}, and Ir^{4+}–Ir^{4+} interactions. When the ferromagnetic phase becomes dominant as the Ir content increases, the specimens with an Ir content of $x \geqslant 0.3$ show ferromagnetism.

Acknowledgments

The work done at Aoyama Gakuin University was supported by The High-Tech Research Center Project for Private Universities with matching fund subsidy from the Ministry of Education, Culture, Sports, Science, and Technology, Japan, 2002–2006. The work accomplished at National Chung Hsing University was supported by the National Science Council of ROC under contract number NSC 95-2112-M-005-010-MY3.

References

[1] Rao C N R and Raveau B 1998 *Colossal Magnetoresistive Oxides are Reviewed in Colossal Magnetoresistance Charge Ordering and Related Properties of Manganese Oxides* (Singapore: World Scientific)
Tokura Y 2000 *Colossal Magnetoresistive Oxides* (New York: Gordon and Breach)
[2] Zeng Z, Greenblatt M and Croft M 1999 *Phys. Rev.* B **59** 8784
[3] Neumeier J J and Cohn J L 2000 *Phys. Rev.* B **61** 14319
[4] Neumeier J J, Cornelius A L and Andres K 2001 *Phys. Rev.* B **64** 172406
[5] Goodenough J B 1999 *Aust. J. Phys.* **52** 155
[6] Loudon J C, Mathur N D and Midgley P A 2004 *J. Magn. Magn. Mater.* **272–276** 13
[7] Savosta M M, Novák P, Englich J, Kohout J, Hejtmánek J and Strej A 2002 *J. Magn. Magn. Mater.* **242–245** 676
[8] Savosta M M, Novák P, Maryško M, Jirák Z, Hejtmánek J, Englich J, Kohout J, Martin C and Raveau B 2000 *Phys. Rev.* B **62** 9532
[9] Dagotto E 2003 *Nanoscale Phase Separation and Colossal Magnetoresistance* (Berlin: Springer) p 456
[10] Martin C, Maignan A, Damay F, Hervieu M, Raveau B and Hejtmánek J 2000 *Eur. Phys. J.* B **16** 469
[11] Vanitha P V, Arulraj A, Raju A R and Rao C N R 1999 *C. R. Acad. Sci.* IIc **2** 595
[12] Raveau B, Maignan A, Martin C and Hervieu M 2000 *Mater. Res. Bull.* **35** 1579
[13] Maignan A, Martin C, Hervieu M and Raveau B 2001 *Solid State Commun.* **117** 377
[14] Pi L, Hebert S, Martin C, Maignan A and Raveau B 2003 *Phys. Rev.* B **67** 024430
[15] Siegrist T and Chamberland B L 1991 *J. Less-Common Met.* **170** 93
[16] Powell A V and Battle P D 1993 *J. Alloys Compounds* **191** 313
[17] Lindsay R, Strange W, Chamberland B L and Moyer R O 1993 *Solid State Commun.* **86** 759
[18] Crawford M K, Subramanian M A, Harlow R L, Fernandez-Baca J A, Wang Z R and Johnston D C 1994 *Phys. Rev.* B **49** 9198
[19] Huang Q, Soubeyroux J L, Chmaissen O, Sora I N, Santoro A, Cava R J, Krajewski J J and Peck W F Jr 1994 *J. Solid State Chem.* **112** 355
[20] Cava R J, Batlogg B, Kiyono K, Takagi H, Krajewski J J, Peck W F Jr, Rupp L W Jr and Chen C H 1994 *Phys. Rev.* B **49** 11890
[21] Fujimori A and Tokura Y 1995 *Spectroscopy of Mott Insulators and Correlated Metals* (Berlin: Springer) p 249
[22] Cao G, Bolivar J, McCall S, Crow J E and Guertin R P 1998 *Phys. Rev.* B **57** R11039
[23] Cao G, Crow J E, Guertin R P, Henning P, Homes C C, Strongin M, Basov D N and Lochner E 2000 *Solid State Commun.* **113** 657
[24] Whangbo M H and Koo H J 2001 *Solid State Commun.* **118** 491
[25] Cao G, Xin Y, Alexander C S, Crow J E and Schlottmann P 2002 *Phys. Rev.* B **66** 214412
[26] Cao G, Lin X N, Chikara S, Durairaj V and Elhami E 2004 *Phys. Rev.* B **69** 174418
[27] Nishimine H, Wakeshima M and Hinatsu Y 2004 *J. Solid State Chem.* **177** 739
[28] Sasaki S *et al* 1983 *Am. Mineral.* **68** 1189
Taguchi H *et al* 1998 *J. Solid State Chem.* **137** 82
Garcia-Jaca J *et al* 1995 *J. Mater. Chem.* **5** 1995
Takeda T *et al* 2000 *Solid State Sci.* **2** 673
Beran A *et al* 1996 *Can. Mineral.* **34** 803
Rama Rao M V *et al* 2001 *J. Phys. Chem. Solids* **62** 797
Rodi F *et al* 1965 *Z. Anorg. Allg. Chem.* **336** 17
Mitchell R H *et al* 1998 *Can. Mineral.* **36** 107
Vallet-Regi M *et al* 1986 *Acta Crystallogr.* C **42** 167
Levin I *et al* 2003 *J. Solid State Chem.* **175** 170
Yamamoto A *et al* 1999 *Chem. Mater.* **11** 747
[29] Shannon R D 1976 *Acta Crystallogr.* A **32** 751
[30] Taniguchi T, Mizusaki S, Okada N, Nagata Y, Lai S H, Lan M D, Hiraoka N, Itou M, Sakurai Y, Ozawa T C, Noro Y and Samata H 2008 *Phys. Rev.* B **77** 014406
[31] Hoppe R and Glaes K 1975 *J. Less-Common Met.* **43** 129
[32] Powell A V, Gore J G and Battle P D 1993 *J. Alloys Compounds* **201** 73
[33] Hayashi K, Demazeeau G, Pouchard M and Hagenmuller P 1980 *Mater. Res. Bull.* **15** 461
[34] Wakeshima M, Harada D and Hinatsu Y 1999 *J. Alloys Compounds* **287** 130
[35] Wakeshima M, Harada D and Hinatsu Y 2000 *J. Mater. Chem.* **10** 419
[36] Goodenough J B 1963 *Magnetism and Chemical Bond* (New York: Wiley) p 168
[37] Matsumoto G 1970 *J. Phys. Soc. Japan* **29** 615
[38] Goodenough J B 1999 *Aust. J. Phys.* **52** 155
[39] de Gennes P G 1960 *Phys. Rev.* **118** 141
[40] Mott N F and Davis E A 1979 *Electronic Process in Non-Crystalline Materials* (Oxford: Clarendon) p 32